3-30-2016

X-ray Absorption Spectroscopy Study of the Effect of Rh Doping in Sr_2IrO_4

C. H. Sohn
Institute for Basic Science (IBS), South Korea

Deok-Yong Cho
Chonbuk National University, South Korea

C. -T. Kuo
Institute for Basic Science (IBS), South Korea

L. J. Sandilands
Institute for Basic Science (IBS), South Korea

Tongfei Qi
University of Kentucky, tongfei.qi@uky.edu

See next page for additional authors

Authors
C. H. Sohn, Deok-Yong Cho, C. -T. Kuo, L. J. Sandilands, Tongfei Qi, Gang Cao, and T. W. Noh

X-ray Absorption Spectroscopy Study of the Effect of Rh Doping in Sr_2IrO_4

Notes/Citation Information
Published in *Scientific Reports*, v. 6, article no. 23856, p. 1-7.

Digital Object Identifier (DOI)
https://doi.org/10.1038/srep23856

SCIENTIFIC REPORTS

OPEN

X-ray Absorption Spectroscopy Study of the Effect of Rh doping in Sr_2IrO_4

Received: 24 October 2014
Accepted: 16 March 2016
Published: 30 March 2016

C. H. Sohn[1,2], Deok-Yong Cho[3], C.-T. Kuo[1,2], L. J. Sandilands[1,2], T. F. Qi[4], G. Cao[4] & T. W. Noh[1,2]

We investigate the effect of Rh doping in Sr_2IrO_4 using X-ray absorption spectroscopy (XAS). We observed appearance of new electron-addition states with increasing Rh concentration (x in $Sr_2Ir_{1-x}Rh_xO_4$) in accordance with the concept of hole doping. The intensity of the hole-induced state is however weak, suggesting weakness of charge transfer (CT) effect and Mott insulating ground states. Also, Ir $J_{eff}=1/2$ upper Hubbard band shifts to lower energy as x increases up to x = 0.23. Combined with optical spectroscopy, these results suggest a hybridisation-related mechanism, in which Rh doping can weaken the (Ir $J_{eff}=1/2$)–(O 2*p*) orbital hybridisation in the in-planar Rh-O-Ir bond networks.

Novel phenomena in 5*d* transition metal oxides (TMOs) have been a central subject in condensed matter physics. The large spin-orbit (SO) coupling transforms the 5*d* electron states from crystal-field-driven orbital states to certain SO-entangled J_{eff} states (J_{eff}: effective total angular momentum)[1,2]. Consequently, a variety of exotic phases, including a relativistic Mott insulator[1–6], a quantum spin liquid[7–11], and a topological insulator[12–14], are shown and expected in 5*d* TMOs. In the case of the most well-known 5*d* TMO, Sr_2IrO_4, even a superconductivity is expected because its crystal structure[15], low energy Hamiltonian[16,17], and magnetic excitation[18,19] are similar to those of the mother compound of high T_C cuprates, La_2CuO_4. Indeed, recent angle-resolved photoemission spectroscopy studies showed the cuprate-like Fermi arc band and the *d*-wave gap in K doped Sr_2IrO_4[20,21].

One of the important issues to be resolved for 5*d* TMOs is how electron/hole doping affects their ground states. It is because the doping behaviours will provide us the clues for understanding emergent phenomena including superconductivity. Studies on $La_{2-x}Sr_xCuO_4$, for instance, manifested a charge transfer ground state where doped holes reside in the ligand O orbitals[22,23]. Such hole states in O 2*p* orbitals form the Zhang-Rice singlet state[24], which has been known as the key component of high T_C superconductivity. Therefore, studies on carrier doping effects on 5*d* TMOs are necessary.

This article focuses on the effect of Rh doping in Sr_2IrO_4. Our Rh *L*-edge X-ray absorption spectroscopy (XAS) study revealed that the valence of Rh at low Rh concentrations is mainly +3 rather than +4, consistent to recent studies[25,26]. Therefore, $Sr_2Ir_{1-x}Rh_xO_4$ can be viewed as hole-doped iridates analogous to hole-doped cuprates. With O *K*-edge XAS, we particularly report two distinct features. One is that a new electron-addition state emerges near the chemical potential as a result of Rh doping. The intensity of the hole-induced states is, however, rather weak compared to the case of cuprates or nickelates. This suggests that the charge transfer (CT) effect is weak and doped holes mainly reside in the Ir 5*d* orbitals, being consistent with known Mott insulating ground state of Sr_2IrO_4. The other feature is that the 5*d* upper Hubbard band (UHB) hybridised with in-plane oxygen (O_p) 2*p* orbitals undergoes a strong redshift whereas the same UHB but hybridised with apical oxygen (O_a) 2*p* orbitals hardly does. We propose that Rh doping can decrease the hybridisation between Ir and O via charge reconstruction in O_p ions and/or via the less extended nature of Rh wave function. Optical spectroscopy study further showed that the onset energy of CT transition from O_p 2*p* to Ir 5*d* indeed decreases with increasing Rh concentration, supporting the interpretation of the XAS results.

Results

Rh L_3-edge XAS was performed to estimate the hole concentration. Figure 1(a) shows the spectra of the $Sr_2Ir_{1-x}Rh_xO_4$ crystals for x = 0.10, 0.23 and 0.41. The peak near 3006 eV corresponds to the L_3-edge white line, which

[1]Center for Correlated Electron Systems, Institute for Basic Science (IBS), Seoul 08826, Korea. [2]Department of Physics and Astronomy, Seoul National University, Seoul 08826, Korea. [3]IPIT & Department of Physics, Chonbuk National University, Jeonju 54896, Korea. [4]Center for Advanced Materials, Department of Physics and Astronomy, University of Kentucky, Lexington, Kentucky 40506, USA. Correspondence and requests for materials should be addressed to D.-Y.C. (email: zax@jbnu.ac.kr) or T.W.N. (email: twnoh@snu.ac.kr)

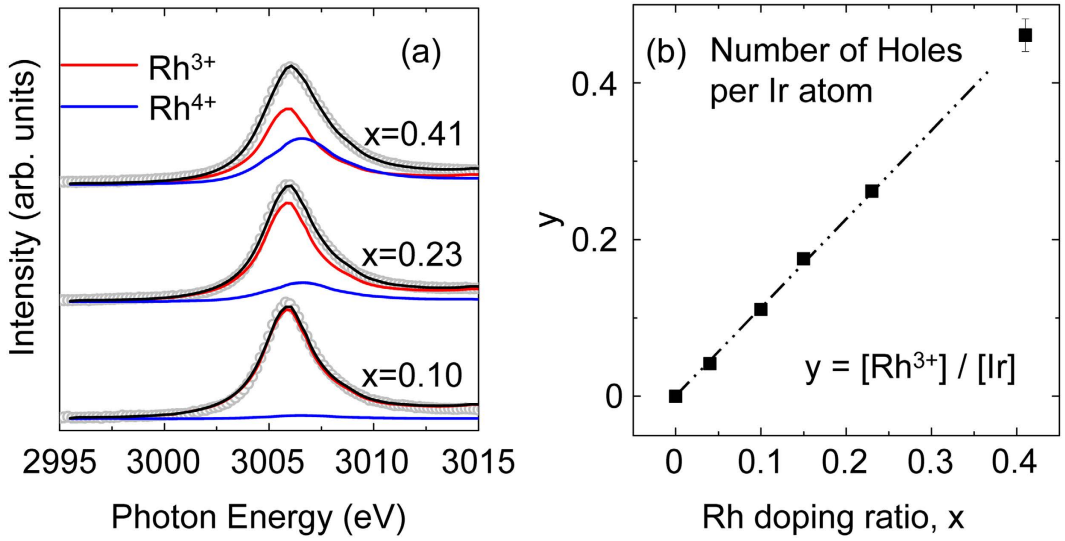

Figure 1. (**a**) Rh L_3-edge XAS spectra of $Sr_2Ir_{1-x}Rh_xO_4$ crystals of x = 0.10, 0.23 and 0.41. The open circles show the experimental spectra and the black solid curves show the fitting results. The spectra of Rh^{3+} in Rh_2O_3 (red curve) and Rh^{4+} in Sr_2RhO_4 (blue curve) were taken from ref. 26 for the fitting. (**b**) The deduced values of Rh^{3+} concentration per one Ir site as a function of Rh doping ratio (x). Almost linear relation manifests the hole doping scheme at least for $x \leq 0.23$. The error bars account for the uncertainty in determining the peak areas.

represents the transitions from Rh $2p_{3/2}$ to 4*d* states. We fitted our spectra to linear combinations of known spectra of Rh^{3+} in Rh_2O_3 (the red lines) and Rh^{4+} in Sr_2RhO_4 (the blue lines)[26]. The valence of Rh is almost +3 rather than +4 in low-x samples ($x \leq 0.23$) while the portion of Rh^{4+} ions starts to be prominent in x = 0.41 sample, consistent with a previous result[26]. Figure 1(b) shows the concentration ratio (y) of dopants to host metal ions ($y = [Rh^{3+}]/[Ir]$), where $[Rh^{3+}]$ is the Rh^{3+} concentration according to our fitting results. It is clearly shown y increases almost linear to x, manifesting the hole doping effect.

The O *K*-edge XAS spectra show that the Rh doping considerably changes the electronic structure of Sr_2IrO_4 near the chemical potential. Figure 2 shows the O *K*-edge XAS spectra of $Sr_2Ir_{1-x}Rh_xO_4$ (x = 0, 0.10, 0.23, 0.41, and 0.71). The spectra near the threshold reflect transitions from O 1*s* core levels to unoccupied O 2*p* states hybridised with Ir/Rh *d* bands. The solid and dashed curves are the XAS spectra taken with σ- and π-polarised light, respectively. The experimental geometry is shown in the inset of Fig. 2. We fixed the angle of the incident beam to be 60°, so the polarisation of σ-polarised light was parallel to the sample surface, while the polarisation of π-polarised light was almost perpendicular to the surface. The huge polarisation dependence in the spectra suggests a quasi-2-dimensional nature in all the samples. With increasing Rh concentration, we observe large and consistent changes in the spectra, especially below the photon energy of 531 eV.

We can assign the peaks below 531 eV as in-plane and apical (O_p and O_a) 2*p* states hybridised with Ir or Rh *d* orbitals, consistent with the previous studies[1,27]. Figure 3 shows the O *K*-edge XAS spectra of $Sr_2Ir_{1-x}Rh_xO_4$ near the threshold with the polarisation vectors (***E***) (a) parallel and (b) perpendicular to the normal axis of the surface (***c*** in the inset of Fig. 2), respectively. In the case of pure Sr_2IrO_4, there exist a single peak near 530.2 eV in the $\boldsymbol{E}//\boldsymbol{c}$ spectrum and a doublet near 529.6 eV and 530.2 eV in the $\boldsymbol{E}\perp\boldsymbol{c}$ spectrum. It is well known that the unoccupied state at lowest energy in Sr_2IrO_4 is close to a singlet of Ir 5*d* $J_{\text{eff}} = 1/2$ UHB, $\frac{1}{\sqrt{3}}(|d_{xy}, \uparrow\rangle + |d_{yz}, \downarrow\rangle + i|d_{zx}, \downarrow\rangle)$. Thus, we attribute the split (of roughly 0.6 eV) as a chemical shift due to different chemistry between O_p and O_a[1,27]. The peaks highlighted by filled triangles in Fig. 3 are the Ir 5*d* UHB hybridised with O_p 2*p* orbitals (UHB_p). Likewise, the peaks marked as open triangles correspond to the Ir 5*d* UHB hybridised with O_a 2*p* orbitals (UHB_a).

With increasing x, we observe appearance of lower-energy peaks, *A* and *B*, as highlighted in Fig. 3. The energies of peaks *A* and *B* are clearly distinct from those of the Sr_2IrO_4 and Sr_2RhO_4 peaks. Such lower-energy peaks are generally shown in hole-doped systems including nickelates[28] or cuprates[22,23], because new electron-addition states appear due to hole doping. Since the energy of such states should be close to that of original occupied states, the difference in energy between UHB and the hole-induced states should roughly reflects the charge gap. We see that the energy difference between peak A and Ir UHB_p (also, between peak *B* and Ir UHB_a) is roughly 0.5 eV, similar to the known value of the charge gap in Sr_2IrO_4. Therefore, peaks *A* and *B* correspond to the electron-addition states hybridised with O_p and O_a orbitals, respectively. The energy difference between peaks *A* and *B* (~0.6 eV) in Fig. 3(b) reflects the difference in chemistry between O_p and O_a, similar to the cases of UHB_p and UHB_a.

Apart from the low-energy peaks (*A* and *B*), it is clearly shown in both Fig. 3(a,b) that the UHB_p peaks shift to lower energy with increasing x. The amount of the UHB_p redshift with respect to the case of undoped iridate is approximately 0.25 eV at x = 0.23. Interestingly, the redshift is much less predominant in the case of UHB_a. Such an anisotropic peak shift in the two peaks is not easy to understand because they share identical Ir 5*d* orbitals ($J_{\text{eff}} = 1/2$ UHB). As will be discussed in the next section, the redshifts are the signatures of reduced O 2*p*–Ir 5*d* hybridisation strength upon the hole doping.

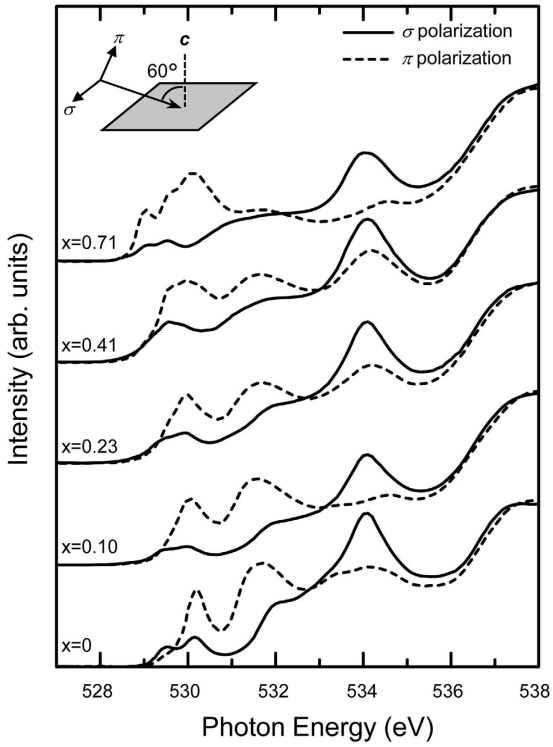

Figure 2. Polarization-dependent O *K*-edge XAS spectra of $Sr_2Ir_{1-x}Rh_xO_4$ crystals. The solid and dashed curves show the spectra taken with σ- and π-polarised light, respectively. The inset shows the measurement geometry.

To conclude this section, we observe two distinct features due to Rh doping in the O *K*-edge spectra: One is the emergence of new electron-addition states (*A* and *B*) at low energy and the other is a concomitant redshift of Ir UHB_p. These will be further analysed in Discussion.

Discussion

To describe the spectral evolution upon Rh doping quantitatively, we fitted the O *K*-edge spectra with ***E***//***c*** using Lorentz-Gaussian models. For $x = 0.04$–0.23 samples, only Rh^{3+} (d^6) prevails so that there could exist three unoccupied states near the chemical potential: the hole-induced states (peak *A*), Ir UHB_p, Rh e_g band with increasing order of energy. Figure 4(a) shows the best fitting result of $x = 0.23$ spectra using the three peaks with a higher energy background for Ir *e_g* band (dashed line). Meanwhile, for highly doped samples ($x \geq 0.41$), it was difficult to obtain reliable fitting results because of the mixed contributions of Rh^{3+} and Rh^{4+} states.

We note that the intensity of peak *A* in Rh doped Sr_2IrO_4 is much smaller than those in cuprates and nickelates. Figure 4(b) shows the areal intensity of peak *A* normalised by that of UHB_p, namely I_A/I_{UHB} of the Rh-doped iridates as a function of y. Small error bars account for the uncertainty in determining the peak intensity. For comparison, we appended the I_A/I_{UHB} values in $(La_{1-x}Sr_x)_2CuO_4$[23] as a function of the number of holes per Cu as well. For the case of the cuprates, I_A/I_{UHB} exceeds 1 even at $y = 0.1$, representatively showing the strong nature of CT insulator. In contrast, I_A/I_{UHB} in Rh doped Sr_2IrO_4 at $y = 0.11$ (or $x = 0.10$), is only approximately 0.14. This indicates that the CT effect in iridates is much weaker compared to that in the cuprates. This observation is consistent with the Mott insulating ground state in Sr_2IrO_4, in which doped holes should reside mainly in metal *d* orbitals rather than ligand orbitals.

Another important finding in the O *K*-edge XAS spectra is that only UHB_p undergoes a redshift whereas UHB_a does not despite they represent the same UHB. Figure 5(a) shows the amount of redshifts (ΔE) of UHB_p and UHB_a with respect to those of undoped Sr_2IrO_4 as a function of y. Only the data for $x \leq 0.23$, which exhibit little secondary phase (Rh^{4+}), are collected. The error bars in the figure account for the uncertainty in determining the peak position through the fitting processes. In order to understand the origin of the redshifts, we first suspect the consistency with the structural evolution. It has been reported that with increasing x, the Ir-O bond is slightly shortened in average and the Ir-O-Ir bonding angle increases in average[29]. This moderate structural distortion would tend to increase the hybridisation strength of the Ir $J_{eff} = 1/2$ UHB–O 2*p* orbitals, which should have resulted in a blueshift of UHB_p or UHB_a. Therefore, structural change upon Rh doping cannot explain the redshifts of UHB.

The plausible mechanism is the decrease of orbital hybridisation in the Ir-O bonds. The energy of UHB can be significantly influenced by the orbital hybridisation of bare Ir $J_{eff} = 1/2$ state and O 2*p* state. The schematic for the orbital hybridisation is illustrated in Fig. 5(b). As a result of the hybridisation, formed are an antibonding state π^*, which is commonly called "Ir UHB", above the chemical potential and a bonding state π, commonly called "O 2*p*",

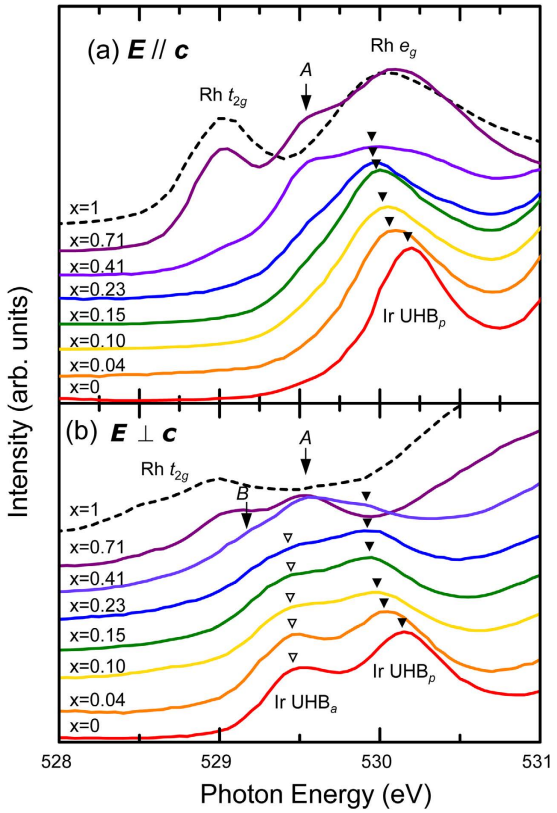

Figure 3. Low energy parts in the O *K*-edge XAS spectra with (**a**) ***E*//*c*** and (**b**) ***E*⊥*c***, where ***c*** is the surface normal axis. The spectra of Sr_2RhO_4 were taken from ref. 27. The ***E*⊥*c*** spectra are reproduced from the σ-polarisation data, and the ***E*//*c*** spectra are deduced from the relation: $I_{E//c} = \frac{I_\pi - \cos^2 60^\circ I_\sigma}{\sin^2 60^\circ}$. Solid (open) triangles highlight the peak positions of the Ir $J_{\rm eff} = 1/2$ UHB hybridised with the in-plane (apical) O 2*p*.

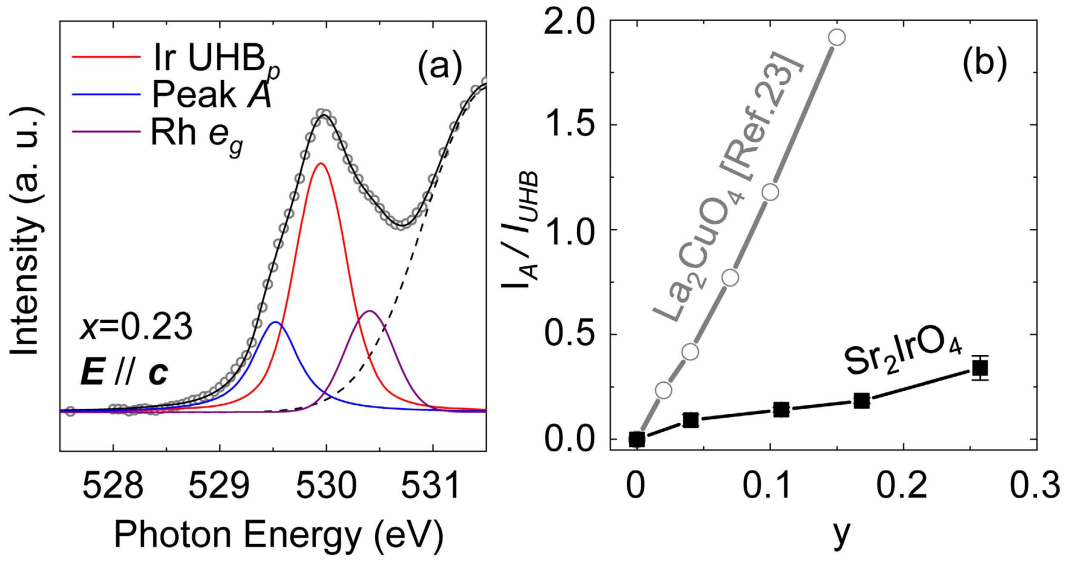

Figure 4. (**a**) The ***E*//*c*** spectra of x = 0.23 sample. The open circles are the experimental data and the black solid line is the fitting result. The red, blue, purple, and dashed curves are for Ir UHB$_p$, peak *A*, Rh e_g, and the Ir e_g background, respectively. (**b**) I_A/I_{UHB} as functions of y (concentration ratio of dopants to host cations). The data of La_2CuO_4 is taken from ref. 23 for the comparison.

below the chemical potential. What is observed in the O *K*-edge XAS data is the lowering of π*(UHB) hybridised with O$_p$ (UHB$_p$). Therefore, the redshift of UHB$_p$ can be easily understood if Rh doping can effectively reduce the

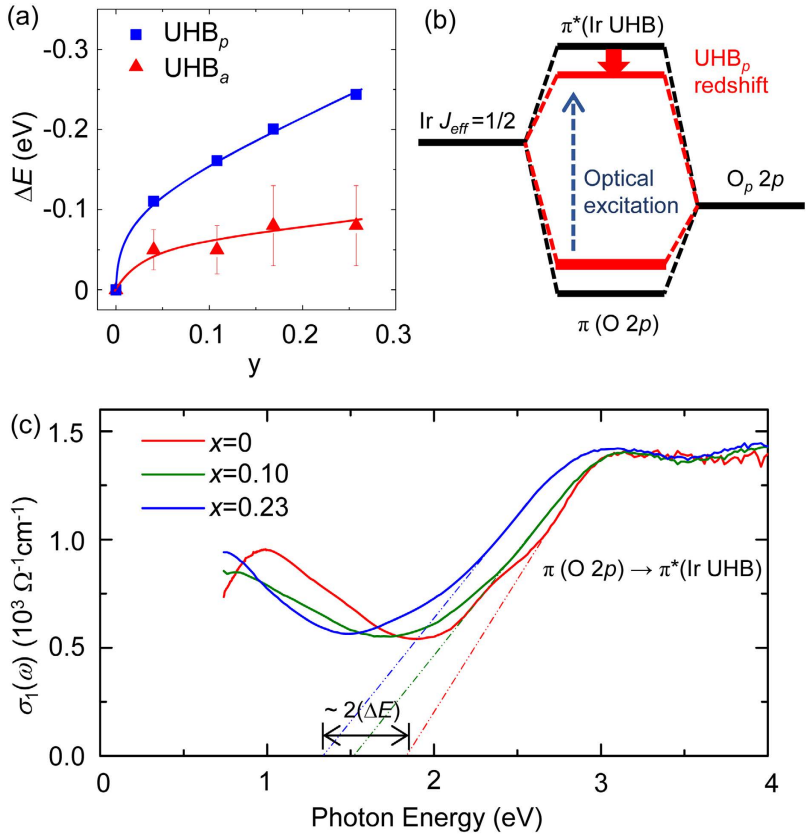

Figure 5. (**a**) Relative peak shifts (ΔE) of UHB_p (squares) and UHB_a (triangles) as functions of y with error bars. The solid lines are guides to the eye. (**b**) Schematic diagram of hybridisation change in Rh doped Sr_2IrO_4. (**c**) $\sigma_1(\omega)$ obtained by optical spectroscopy. The extrapolations toward the abscissa roughly visualize the onsets of the charge transfer excitations from in-plane O 2*p* to Ir 5*d* UHB.

orbital hybridisation. This mechanism is more effective in the in-planar directions because the influence of Rh can reach Ir only via the in-plane O, namely, through Rh-O_p-Ir bond chains due to quasi-2-dimensional crystal structure of Sr_2IrO_4. This explains why UHB_p suffers much more intense redshift compared to UHB_a (see Fig. 5(a)).

We propose two possible microscopic origins how Rh doping can decrease the orbital hybridisation between Ir *d* and O 2*p* orbitals. One is related to the difference of valence of ions. When the iridate is doped with Rh^{3+} ions, charge redistribution in O_p ions occurs: Since Rh can supply only 3 electrons to the O_p ions, O_p tend to attract more electrons from neighbouring Ir ions. It effectively increases the electronegativity of O_p in Ir-O_p bond, thereby making the Ir-O_p bond ionic. Similar mechanism but opposite trend has been discussed in H doped VO_2[30]. The enhanced ionic character of the Ir-O_p bond can decrease hybridisation between two ions. The other is related to the less extended nature of Rh wave functions. According to the results of previous dynamical mean-field theory calculations, hybridisation between Ir and O ions is much stronger than that between Rh and O ions[31]. Because the valence *d* orbitals comprise the admixture of Ir and Rh *d* orbitals, Rh doping can effectively decrease the hybridisation between Ir 5*d* and O 2*p* orbitals.

To support the hybridisation mechanism discussed above, we measured the difference in energy between π and π^* using optical spectroscopy. Figure 5(c) shows the in-plane real part of optical conductivity $\sigma_1(\omega)$ of the x = 0, 0.10, and 0.23 samples. According to a previous study[32], the broad features above photon energy of 2.5 eV can be attributed to a charge excitation from π (O 2*p*) to π^* (Ir UHB). Meanwhile, the broad peak near 1 eV and the bump near 2.3 eV can be attributed to Ir *d*-*d* transition, which is less relevant to the main interest in this work. It is clearly observed that the onset energy of the high energy bump decreases with increasing x. This suggests that the Ir UHB–O 2*p* hybridisation becomes weaker as the hole doping is promoted, consistent with our XAS observations and interpretations.

The energy differences between π and π^* bands can be roughly estimated from the extrapolations toward the abscissa. Compared to the case of undoped Sr_2IrO_4, the onset energy of x = 0.23 (x = 0.10) decreased by approximately 0.5 eV (0.3 eV), which is about two times larger than the amount of the UHB_p redshift (shown in Fig. 5(a)). This is consistent with the hybridisation mechanism for weakened hybridisation not only lowers the π^* band but also lifts up the π band by similar magnitude. Therefore, $\sigma_1(\omega)$ data supports the hybridisation mechanism for the UHB redshifts.

It is worthwhile to consider the consequence of reduced Ir UHB–O 2*p* hybridisation due to Rh doping on the low-energy physics in Sr_2IrO_4. It is well known that the low energy physics in strongly correlated electron systems can be largely determined by the ratio of on-site Coulomb interaction (*U*) to the single electron bandwidth (*W*).

According to the results of a recent *ab initio* calculation, the value of U would decrease due to enhanced ligand screening[31] so that U/W should decrease altering the electronic structure near the bandgap. However, the results of recent angle-resolved photoemission experiment show that Rh doping induces only a rigid shift of bands without an appreciable change in band dispersions[33]. This controversy can be resolved by noting that the value of W should decrease as well, because the decrease in hybridisation strength (by Rh doping) will reduce the bandwidth of the UHB. Therefore, the value of U/W should not change substantially.

In conclusion, Rh doped Sr_2IrO_4 exhibit peculiar evolution in electronic structure: i) a charge transfer state emerges near the chemical potential but the feature is not that strong as in the hole-doped cuprate, consistent to the Mott insulating ground state, and ii) the Ir UHB energy is lowered by a few tenths eV due to reduced Ir $J_{\rm eff} = 1/2$ UHB–O $2p$ hybridisation strength upon the hole doping.

Methods

Materials. High-quality single crystals $Sr_2Ir_{1-x}Rh_xO_4$ ($0 \le x \le 0.71$) were synthesized from off-stoichiometric quantities of $SrCl_2$, $SrCO_3$, IrO_2, and RhO_2 using self-flux method. Detailed methods are described elsewhere[29].

X-ray absorption spectroscopy. Polarization-dependent O K-edge X-ray absorption spectroscopy (XAS) was performed at the 2A beamline of the Pohang Light Source in total electron yield mode. To obtain a clean surface, we cleaved samples *in situ* in an ultra-high vacuum (~6×10^{-8} Pa). We fixed the angle of the incident beam as 60 degrees, and changed the direction of polarisation to resolve the in- and out-of-plane O responses. Rh L-edge XAS was performed at the 16A1 beamline of the National Synchrotron Radiation Research Center in Taiwan in fluorescence yield mode. All the XAS spectra were collected at room temperature.

Optical spectroscopy. We performed ellipsometry measurement to obtain the real part of optical conductivity between 0.74 and 4 eV at room temperature using a V-VASE ellipsometer (J. A. Woollam Co.).

References

1. Kim, B. J. *et al.* Novel $J_{\rm eff} = 1/2$ Mott State Induced by Relativistic Spin-Orbit Coupling in Sr_2IrO_4. *Phys. Rev. Lett.* **101,** 076402 (2008).
2. Kim, B. J. *et al.* Phase-Sensitive Observation of a Spin-Orbital Mott State in Sr_2IrO_4. *Science* **323,** 1329–1332 (2009).
3. Moon, S. J. *et al.* Dimensionality-Controlled Insulator-Metal Transition and Correlated Metallic State in 5*d* Transition Metal Oxides $Sr_{n+1}Ir_nO_{3n+1}$ ($n = 1, 2$, and ∞). *Phys. Rev. Lett.* **101,** 226402 (2008).
4. Okabe, H. *et al.* Ba_2IrO_4: A spin-orbit Mott insulating quasi-two-dimensional antiferromagnet. *Phys. Rev. B* **83,** 155118 (2011).
5. Comin, R. *et al.* Na_2IrO_3 as a Novel Relativistic Mott Insulator with a 340-meV Gap. *Phys. Rev. Lett.* **109,** 266406 (2012).
6. Ohgushi, K. *et al.* Resonant X-ray Diffraction Study of the Strongly Spin-Orbit-Coupled Mott Insulator $CaIrO_3$. *Phys. Rev. Lett.* **110,** 217212 (2013).
7. Chaloupka, J., Jackeli, G. & Khaliullin, G. Kitaev-Heisenberg Model on a Honeycomb Lattice: Possible Exotic Phases in Iridium Oxides A_2IrO_3. *Phys. Rev. Lett.* **105,** 027204 (2010).
8. Singh, Y. *et al.* Relevance of the Heisenberg-Kitaev Model for the Honeycomb Lattice Iridates A_2IrO_3. *Phys. Rev. Lett.* **108,** 127203 (2012).
9. Chaloupka, J., Jackeli, G. & Khaliullin, G. Zigzag Magnetic Order in the Iridium Oxide Na_2IrO_3. *Phys. Rev. Lett.* **110,** 097204 (2013).
10. Cao, G. *et al.* Evolution of magnetism in the single-crystal honeycomb iridates $(Na_{1-x}Li_x)_2IrO_3$. *Phys. Rev. B* **88,** 220414(R) (2013).
11. Takayama, T. *et al.* Spin-orbit coupling induced semi-metallic state in the 1/3 hole doped hyper-kagome $Na_3Ir_3O_8$. *Sci. Rep.* **4,** 6818 (2014).
12. Shitade, A. *et al.* Quantum Spin Hall Effect in a Transition Metal Oxide Na_2IrO_3. *Phys. Rev. Lett.* **102,** 256403 (2009).
13. Kim, C. H., Kim, H.-S., Jeong, H., Jin, H. & Yu, J. Topological Quantum Phase Transition in 5*d* Transition Metal Oxide Na_2IrO_3. *Phys. Rev. Lett.* **108,** 106401 (2012).
14. Kim, H.-S., Kim, C. H., Jeong, H., Jin, H. & Yu, J. Strain-induced topological insulator phase and effective magnetic interactions in Li_2IrO_3. *Phys. Rev. B* **87,** 165117 (2013).
15. Crawford, M. K. *et al.* Structural and magnetic studies of Sr_2IrO_4. *Phys. Rev. B* **49,** 9198–9201 (1994).
16. Wang, F. & Senthil, T. Twisted Hubbard Model for Sr_2IrO_4: Magnetism and Possible High Temperature Superconductivity. *Phys. Rev. Lett.* **106,** 136402 (2011).
17. Watanabe, H., Shirakawa, T. & Yunoki, S. Monte Carlo Study of an Unconventional Superconducting Phase in Iridium Oxide $J_{\rm eff} = 1/2$ Mott Insulators Induced by Carrier Doping. *Phys. Rev. Lett.* **110,** 027002 (2013).
18. Kim, J. *et al.* Magnetic Excitation Spectra of Sr_2IrO_4 Probed by Resonant Inelastic X-Ray Scattering: Establishing Links to Cuprate Superconductors. *Phys. Rev. Lett.* **108,** 177003 (2012).
19. Kim, J. *et al.* Excitonic quasiparticles in a spin–orbit Mott insulator. *Nat. Commun.* **5,** 4453 (2014).
20. Kim, Y. K. *et al.* Fermi arcs in a doped pseudospin-1/2 Heisenberg antiferromagnet. *Science* **345,** 187–190 (2014).
21. Kim, Y. K., Sung, N. H., Denlinger., J. D. & Kim, B. J. Observation of a *d*-wave gap in electron-doped Sr_2IrO_4. *Nat. Phys.* **12,** 37–41 (2016).
22. Nücker, N., Fink, J., Fuggle, J. C., Durham, P. J. & Temmerman, W. M. Evidence for holes on oxygen sites in the high-T_c superconductors $La_{2-x}Sr_xCuO_4$ and $YBa_2Cu_3O_{7-y}$. *Phys. Rev. B* **37,** 5158–5163 (1988).
23. Chen, C. T. *et al.* Electronic states in $La_{2-x}Sr_xCuO_{4+\delta}$ probed by soft-x-ray absorption. *Phys. Rev. Lett.* **66,** 104–107 (1991).
24. Zhang, F. C. & Rice, T. M. Effective Hamiltonian for the superconducting Cu oxides. *Phys. Rev. B* **37,** 3759–3761 (1988).
25. Klein, Y. & Terasaki, I. Insight on the electronic state of Sr_2IrO_4 revealed by cationic substitutions. *J. Phys.: Condens. Matter* **20,** 295201 (2008).
26. Clancy, J. P. *et al.* Dilute magnetism and spin-orbital percolation effects in $Sr_2Ir_{1-x}Rh_xO_4$. *Phys. Rev. B* **89,** 054409 (2014).
27. Moon, S. J. *et al.* Electronic structures of layered perovskite Sr_2MO_4 (M = Ru, Rh, and Ir). *Phys. Rev. B* **74,** 113104 (2006).
28. Kuiper, P., Kruisinga, G., Ghijsen, J., Sawatzky, G. A. & Verweij, H. Character of holes in $Li_xNi_{1-x}O$ and their magnetic behavior. *Phys. Rev. Lett.* **62,** 221–224 (1989).
29. Qi, T. F. *et al.* Spin-orbit tuned metal-insulator transitions in single-crystal $Sr_2Ir_{1-x}Rh_xO_4$ ($0 \le x \le 1$). *Phys. Rev. B* **86,** 125105 (2012).
30. Filinchuk, Y. *et al. In situ* diffraction study of catalytic hydrogenation of VO_2: Stable phases and origins of metallicity. *J. Am. Chem. Soc.* **136,** 8100–8109 (2014).
31. Sohn, C. H. *et al.* Orbital-Dependent Polaron Formation in the Relativistic Mott Insulator Sr_2IrO_4. *Phys. Rev. B* **90,** 041105(R) (2014).
32. Martins, C., Aichhorn, M., Vaugier, L. & Biermann., S. Reduced effective spin-orbital degeneracy and spin-orbital ordering in paramagnetic transition-metal oxides: Sr_2IrO_4 versus Sr_2RhO_4. *Phys. Rev. Lett.* **107,** 266404 (2011).
33. Cao, Y. *et al.* Hallmarks of the Mott-Metal Crossover in the Hole Doped $J = 1/2$ Mott insulator Sr_2IrO_4. *arXiv*:1406.4978.

Acknowledgements

We thank L.-Y. Jang and B.-J. Su for assisting Rh *L*-edge x-ray absorption spectroscopy and H.D. Kim and C.H. Kim for fruitful discussion. This work was supported by IBS-R009-D1. D.-Y.C. acknowledges support from Basic Science Research Program through the National Research Foundation of Korea funded by the Ministry of Science, ICT and Future Planning (NRF-2015R1C1A1A02037514). G.C. acknowledges support by the U.S. National Science Foundation via Grant No. DMR-1265162.

Author Contributions

C.H.S. and D.-Y.C. conceived the experiments, and C.H.S., D.-Y.C. and C.-T.K. performed the XAS measurements. L.J.S. performed the optical measurement. T.F.Q. and G.C. fabricated the crystals. D.-Y.C. and T.W.N. supervised the research. All authors contributed to the writing of the manuscript.

Additional Information

Competing financial interests: The authors declare no competing financial interests.

How to cite this article: Sohn, C. H. *et al.* X-ray Absorption Spectroscopy Study of the Effect of Rh doping in Sr_2IrO_4. *Sci. Rep.* **6**, 23856; doi: 10.1038/srep23856 (2016).